Error analysis for global positioning system network

M. R. Mostsfs[a], H. El-Ghazouly[a], A. Tealeb[b] and M. Salem Abd El-Gelil[b]
[a] *Transportation Dept., Faculty of Eng., Alexandria University, Alexandria, Egypt*
[b] *National Research Institute of Astronomy and Geophysics, Helwan, Cairo, Egypt*

The main objective of this paper is to study the influence of some errors effecting GPS observation on a geodetic network established in 1994 in the area surrounding the Gulf of Suez, the south and the middle of Sinai Peninsula. This network was firstly measured three times in 1994, 1995, and 1996 using Trimble 4000 SSE receivers. The date concerning the year 1996 campaign was taken and processed to study the effect of errors on precision for ten baselines with different lengths and in different days during the observation period. Secondly, a comparison study was made between the broadcast and the precise ephemeredes and their effect on the standard deviation values. Thirdly a model for tropospheric delay such as Hopfield model was used to study the effect of using such a model or ignoring it. Also, different elevation mask angles were used. From this paper it was found that precise ephemeredes was very accurate compares to the broadcast ephemeredes especially for lengths more than 150 km. It was proven that dealing with tropospheric effect by using model is highly advocated for high accuracy application. Finally, results showing that in case the estimated zenith delay state equals zero, in addition to increasing the period of measurements applying session time fixed for all baselines and campaign will improve the results.

يهتم هذا البحث بالدراسة الفعلية للأخطاء على شبكة جيوديسية ثم إنشاؤها في عام ١٩٩٤ حول خليج السويس وجنوب ووسط جزيرة سيناء وقد تم رصد هذه الشبكة فى أعوام ١٩٩٤،١٩٩٥،١٩٩٦ على التوالي وقد تمت الدراسة على الأرصاد التي تمت عام ١٩٩٦ وذلك لمقارنة تأثير المدارات الدقيقة والمدارات المذاعة وكذلك استخدام نموذج رياضي للتعامل مع التروبوسفير لدراسة جدوى استخدام هذا النموذج من عدمه بالإضافة إلى استخدام زوايا ارتفاع مختلفة وقد انتهى البحث إلى أن استخدام المدارات الدقيقة يعطى دقة أكبر من استخدام المدارات المذاعة فى الأطوال أكثر من ١٥٠ كم. كما انتهى البحث أيضا الى أن عدم استخدام نموذج رياضي للتعبير عن التأخير الناتج من التروبوسفير يعطى نتائج بعيدة عن الحقيقة مع التوصية بجعل وقت الرصد للشبكة جميعها متساوي للحصول على دقة متقاربة. كذلك أظهرت النتائج أنه عند جعل (Estimated Zenith Delay State) يساوى صفر يمكن الحصول على نتائج أفضل كما أن زيادة فترات الرصد يحسن كثيرا فى النتائج.

Keywords: GPS, Orbital errors, Code pseudo range, Atmosphere, Hopfield model.

1. Introduction

GPS measurements like most geodetic measurements from space are based on the propagation of electromagnetic waves through the atmosphere. So that, variation in the refractive index of the atmosphere causes changes in the velocity, frequency, and direction of electromagnetic waves propagating through it.

Therefore corrections must be applied to the measured parameters, to account for the effect of the atmosphere. This paper is basically devoted to investigate the influence of troposphere, orbital errors and elevation mask angle on geodetic networks precision. A GPS geodetic network (from the National Research Institute of Astronomy and Geophysics (NRIAG)) consisting of 12-observation stations was established to monitor the horizontal displacements around Sinai Peninsula Red Sea region. This Network was measured three times by Trimble 4000 SSE receivers. Data of 1996 campaign are taken and processed to study practically the effect of troposphere and orbital errors on the precise ephemeredes and their effect on the standard deviation values.

2. Observation equations

In principle, there are two basic observable to determine one's position using GPS. Firstly, the phase observable which is the most important for precise geodetic applications. In a two receiver's configuration, it gives accurate relative position information. Secondly, the code observable, which provides information that is not accurate, enough for surveying application, where sub-meter accuracy is required. However, it can be used in addition to the phase observable [1, 2, 3].

2.1. Code pseudo range

This type of observable is a measure of the relative time between the satellite and receiver clock epochs, including signal transit time. Let us denote t^S the reading of the satellite clock at emission time (according to satellite time scale), and t_R the reading of receiver clock at signal reception time (according to receiver time scale). In addition to the satellite and receiver time scales, there is more or less ideal time scale called GPS time $t_{(GPS)}$, the difference between the clock readings is equivalent to the time shift Δt [4].

$$\left.\begin{aligned} \Delta t &= t_R - t^S \\ \Delta t &= \left[t_{R(GPS)} - \delta_R\right] - \left[t^S_{(GPS)} - \delta^S\right] \\ &= \Delta t_{(GPS)} + \left(\delta^S - \delta_R\right) \end{aligned}\right\}, \quad (1)$$

where,

$$\Delta t_{(GPS)} = t_{R(GPS)} - t^S_{(GPS)}, \text{ and} \quad (2)$$

$$\Delta\delta = \delta^S - \delta_R ,$$

where δ^S is the bias of the satellite clock, and δ_R is the receiver clock delay. The time interval Δt multiplied by the speed of light c yields the pseudo range,

$$\left.\begin{aligned} \text{Range} &= c.\,\Delta t \\ &= c.\Delta t_{(GPS)} + c.\Delta\,\delta \\ &= \rho + c.\Delta\,\delta \end{aligned}\right\} . \quad (3)$$

Where ρ is the true distance between the satellite position at epoch t^S (GPS) and the position of receiver's antenna at epoch t_R (GPS). The receiver coordinates are hidden in the geometric range ρ [5,6].

$$\rho = \sqrt{(x^S - x_R)^2 + (y^S - y_R)^2 + (z^S - z_R)^2} \quad , \quad (4)$$

in which x^S, y^S, and z^S are the satellite coordinates with respect to WGS 84. x_R, y_R, and z_R are the antenna coordinates with respect to WGS 84.

In eq. (3) no biases are considered. However, in reality, there are biases due to the earth's atmosphere (ionosphere and troposphere). Considering these biases another terms can be added to represent some biases such as; (ionosphere, troposphere, noise, ...etc.). eq. (3) will be:

$$\text{Range}=\rho + d\rho + c.(t^S - t_R) + d^{Iono} + d^{Trop} + \varepsilon(R), \quad (5)$$

where:

$d\rho$	is the nominal (broadcast) orbital error component and orbital error component due to selective availability
d^{Iono}, d^{Trop}	is the ionospheric and tropospheric delays, respectively,
$\varepsilon(R)$	is the receiver code measuring noise (function of receiver components, tracking bandwidth, and code).

2.2. Phase pseudo range

The instantaneous circular frequency f is defined by the derivation of the phase φ with respect to time [2],

$$f = \frac{d\varphi}{dt} . \quad (6)$$

The phase is obtained from integration of the frequency between the epochs' t_0 and t.

$$\varphi = \int_{t_0}^{t} f.dt \cdot \quad (7)$$

If the frequency is constant, initial phase $\varphi(t_0)=0$, and taking into account the time span t_l which the signal needs to propagate through the distance (L) from the emitter to the receiver. The phase equation can be obtained as follows:

$$\varphi = f.(t - t_l) = f\left(t - \frac{\rho}{c}\right). \quad (8)$$

Let us denote by φ^S (t) the phase of the received carrier with frequency f^S and by $\varphi_R(t)$ the phase of the reference carrier generated in the receiver with frequency f_R. According to eq. (8) the following phase equations are obtained,

$$\varphi^S(t) = f^S.t - f^S.\frac{\rho}{c} - \varphi_0^S \quad \text{, and} \quad (9)$$

$$\varphi_R(t) = f_R.t - \varphi_{0R} \cdot \quad (10)$$

Where, $\varphi_0^S(t)$ and φ_{0R} are the initial phases and are caused by clock errors for satellite and receiver, respectively, and

$$\varphi_0^S = f^S.\delta^S \text{ And } \varphi_{0R} = f_R.\delta_R \cdot \quad (11)$$

Hence, the beat phase $\varphi_R^S(t)$ is given by:

$$\varphi_R^S(t) = \varphi^S(t) - \varphi_R(t) = -f^S.\frac{\rho}{c} - f^S.\delta^S + f_R.\delta_R + \left(f^S - f_R\right)t \quad (12)$$

The deviation of the frequencies f_S, f_R from the nominal frequency f is only in the order of some fractional parts of Hz, thus, one can assume that $f_S = F_R$. Eq. (12) can be written in amore simple form:

$$\varphi_R^S(t) = -f.\frac{\rho}{c} - f.\Delta\delta \cdot \quad (13)$$

Eq. (13) is the carrier beat phase model but for ideal earth (no atmospheric effect). If ionospheric and tropospheric effects are added to eq. (13) then:

$$\varphi_R^S(t) = -f.\frac{\rho}{c} - f.\Delta\delta - \frac{f}{c}.\left(-d^{Iono} + d^{Trop}\right). \quad (14)$$

In practice, the carrier beat phase measurement at some epoch t is based on phase alignment of the receiver clock with the incoming carrier signal without the knowledge of which cycle would represent perfect cycle synchronization. Hence, the total phase ϕ_{total} consists of a measured fractional part Fr (ϕ), an integer count Int (ϕ) of phase cycles from the initial epoch to epoch t (which is continuously monitored by the receiver since the first measurement), and as unknown integer number N of cycles at the initial epoch t_0 [7]

$$\phi_{total} = Fr(\phi) + Int(\phi; t_0, t) + N(t_0). \quad (15)$$

Denoting the receiver observation by $\phi_{measured}$

$$\phi_{measured} = Fr(\phi) + Int(\phi; t_0, t). \quad (16)$$

$$\phi_{total} = \phi_{measured} + N(t_0). \quad (17)$$

Putting

$$\Phi = -\lambda.\phi_{measured}$$

$$\Phi = \left(\frac{f}{c}\right)\cdot\rho + f\cdot\Delta\delta + \left(\frac{f}{c}\right)\cdot\left(-d^{Iono} + d^{Trop}\right) + N, \quad (18)$$

by multiplying this equation by wavelength λ:

$$\Phi = \rho + c\cdot\Delta\delta - d^{Iono} + d^{Trop} + \lambda\cdot N, \quad (19)$$

Adding the noise in the above equation, then the basic function is [8]

$$\Phi = \rho + c\cdot\Delta\delta - d^{Iono} + d^{Trop} + \lambda\cdot N + \varepsilon(\Phi). \quad (20)$$

Where $\varepsilon(\Phi)$ is receiver measuring noise and function of receiver components, and tracking bandwidth.

3. Errors in GPS

The code pseudo ranges (eq. (3)), and phase pseudo ranges (eq. (20)), are affected by both systematic errors or biases and random noise. The error sources can be classified into three groups, namely satellite related errors, propagation medium related errors, and receiver related errors. The systematic errors can be modeled and give rise to additional terms in the observation equations (e.g. troposphere) which will be explained as an example. Also, the effect of orbital type will be explained and its effect will be studied.

3.1. The neutral atmosphere

The neutral (non-ionized) atmosphere is an approximately spherical shell extending outward from the earth's surface to about 100 km above it. The lower part of this shell, ranging from the surface of the earth to approximately 50 km above it, contains about 99.9% of all the atmospheric mass, [9]. It consists of the troposphere (0-10 km), in which temperature decreases with height, the tropopause (10 km), in which temperature remains constant, and the stratosphere (10-50 km), in which temperature increases with height.

3.2. Tropospheric delays

The tropospheric delay experienced by an electromagnetically measured distance is given by, (e.g. [10])

$$d^{Trop} = \int_{\substack{\text{signal}\\ \text{path}}} n \cdot dL - \int_{\substack{\text{geometric}\\ \text{path}}} ds \ , \qquad (21)$$

where:

d^{Trop} is the Tropospheric delay in meters ,

n is the Index of refraction along the path of signal.

If signal path bending is small, the first integral in eq. (21) can also be taken along the geometric path:

$$d^{Trop} = \int_{\substack{\text{geometric}\\ \text{path}}} (n-1) \cdot ds \ . \qquad (22)$$

Usually, instead of the refractive index n the refractivity N^{Trop} is used:

$$d^{Trop} = 10^{-6} \cdot \int_{\substack{\text{geometric}\\ \text{path}}} N^{Trop} \cdot ds \ . \qquad (23)$$

The tropospheric delay is a function of the distance traveled by the electromagnetic signal through the neutral atmosphere. The distance to be traveled by the signal before reaching the observing station is a function of the elevation of the satellite. Therefore, the tropospheric delay for a satellite at elevation E_v is often written as the product of the delay at zenith (E_v = 90) and a mapping function which relates this zenith delay to the delay at elevation E_v:

$$d^{Trop}(E_v) = F(E_v, \underline{P}) \cdot d^{Trop}(90^\circ) \ . \qquad (24)$$

In which $F(E_v, \underline{P})$ is the mapping function to relate the zenith delay to $d^{Trop}(E_v)$. It is always a function of elevation; sometimes it is also a function of other parameters, contained in the vector $\underline{P}$. Note that $F(90, \underline{P})$ should be equal to one.

The water vapor content becomes zero at a height of 10 km. The dry air content at this height is still about one third of its surface value [3]. It is therefore convenient to write the tropospheric refractive index as the sum of a "dry" and a "wet" component:

$$N^{Trop} = N_d^{Trop} + N_w^{Trop} \ , \qquad (25)$$

where the dry part results from the dry atmosphere and the wet part results from the water vapor. Correspondingly, we have the relations:

$$d_d^{Trop} = 10^{-6} \cdot \int N_d^{Trop} \cdot ds \ , \qquad (26)$$

$$d_w^{Trop} = 10^{-6} \cdot \int N_w^{Trop} \cdot ds \text{ , and} \quad (27)$$

$$d^{Trop} = d_d^{Trop} + d_w^{Trop} \quad (28)$$

$$= 10^{-6} \cdot \int N_d^{Trop} \cdot ds + 10^{-6} \cdot \int N_w^{Trop} \cdot ds \,. \quad (29)$$

3.3. Refractivity

According to [12], for frequencies up to 20 GHz, the refractivity N of moist air is given by [13]:

$$N = k_1 \cdot \frac{p_d}{T} \cdot Z_d^{-1} + k_2 \cdot \frac{e}{T} \cdot Z_w^{-1} + k_3 \cdot \frac{e}{T^2} \cdot Z_w^{-1} \,. \quad (30)$$

Where:

p_d is the partial pressure of dry air (mbar),

e is the partial pressure of water vapor (mbar),

T is the temperature (Kelvin),

k_1, k_2, k_3 are the empirically determined constants with units (k/mbar), (k/mbar) and (k/mbar^2), respectively,

Z_d^{-1} is the inverse compressibility of dry air, and

Z_w^{-1} is the Inverse compressibility of wet air.

Referring to eq. (25), the first term on the right hand side of eq. (30) is the dry refractivity N_d, whereas, the last two terms form the wet refractivity N_w. In radio meteorology eq. (30) is most often rewritten in the form [14]:

$$N = k_1 \cdot \frac{p}{T} \cdot Z_d^{-1} + k_2' \cdot \frac{e}{T^2} \cdot Z_w^{-1} \,. \quad (31)$$

Where:

$$k_2' = [(k_2 - k_1) \cdot T + k_3] \,. \quad (32)$$

The first and second terms of eq. (32) are commonly referred to as the "dry" and "wet" components of refractivity. Under normal circumstances (p_d=1000 mbar, e=10 mbar, T = 273 k) Z_d^{-1} and Z_w^{-1} are close to unity. Therefore, in most other models of refractivity, ideal gas behavior is assumed and the inverse compressibility have a constant value equal to one. Many investigators have determined the constants k_1, k_2, and k_3, but the values, which was recommended by [15] are widely used. However, the International Association of Geodesy (IAG) recommended using the values derived by Essen and Froome.

Therefore, both sets of constants, together with these derived by [12], are given in table 1.

The values for k_1, k_2, and k_3, as mentioned above, are empirically determined and, certainly, cannot fully describe the local situation. An improvement is obtained by measuring meteorological data at the observation site. The following paragraphs present several models when meteorological surface data are taken into account.

3. 4. Hopfield model

Hopfield model employs the dry and wet refractivity component definition as expressed in eq. (29). The dry atmosphere is approximated by a single polytropic layer extending from the surface to an altitude of approximately 40 km. as shown in fig. 1. The dry refractivity profile is given as:

Table 1
Some possible values for the constants k_1, k_2, k_3

Source	k_1 (k/mbar)	k_2 (k/mbar)	k_3 (k/mbar^2)
Smith and Weintraub	77.607	71.6	$3.747.10^5$
Essen and Froome	77.624	64.7	$3.197.10^5$
Thayer	77.604	64.8	$3.776.10^5$

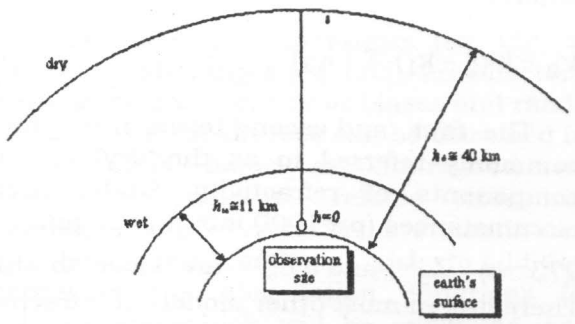

Fig. 1. Thickness of polytropic layers for the troposphere.

$$N_d^{Trop}(h) = N_{d,o}\left[\frac{h_d - h}{h_d}\right]^u . \quad (33)$$

Typical values for the exponent u and dry component scale height h_d is given from [9]. u = 4, and h_d = 40136+148.72(T-273.16).

Substitution of u and h_d assuming that the delay is calculated along a vertical direction, neglecting the curvature of the signal path (fig. 1), the integral can be solved. Then, substituting (h = 0.0) for other observation site on the earth's surface, the dry portion of the troposphere can be obtained as:

$$d_d^{Trop} = \frac{N_{d,o}^{Trop} \cdot h_d}{5 * 10^6} . \quad (34)$$

The wet portion of the troposphere is much more difficult to model because of the variations of the water vapor with respect to space and time. However, Hopfield assumed the same functional model for both the wet and dry components because of the lack of an appropriate alternative. Thus N_w^{Trop} is given as:

$$N_w^{Trop} = N_{w,o}^{Trop}\left[\frac{h_w - h}{h_w}\right]^4 . \quad (35)$$

Where h_w values ranged from 8.5 to 15 km above the earth's surface, using a mean value of h_w equal 11 km, the wet portion of the troposphere can be represented as:

$$d_w^{Trop} = \frac{N_{w,o}^{Trop} \cdot h_w}{5 * 10^6} . \quad (36)$$

Finally, the total tropospheric path delay in meters, can be expressed as:

$$d^{Trop} = 0.2 * 10^{-6}\left(N_{d,o}^{Trop} \cdot h_d + N_{w,o}^{Trop} \cdot h_w\right). \quad (37)$$

4. Practical study

A practical study was carried out on the geodetic network of the Gulf of Suez and Sinai area. The geodetic network is shown in fig. 2. It covers a geographical area located within latitude 27° 20′, 30° 40′ and longitude 32° 10′, 34° 30′. The network consists of 12 observation stations distributed along this area, and the geodetic coordinates are shown in table 2 in WGS 84 coordinate system. The baselines, which were observed, range from 53 km to 245 km. This network covers east, west Gulf of Suez, and middle, south Sinai Peninsula [16, 17].

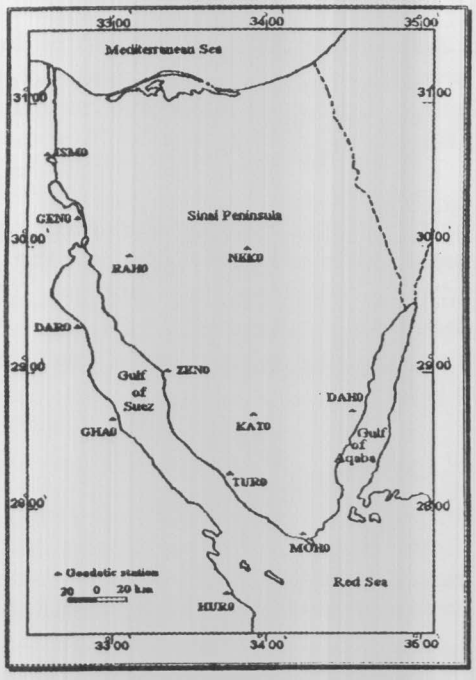

Fig. 2. Geodetic netwok for Sinai Peninsula and Gulf of Suez.

4.1. GPS data analysis

4.1.1. Selected data

Ten baselines were selected from the 29 baselines, which were observed. These baselines' lengths sample represents the baselines in the whole network and covers all directions and days of the campaign. Seven baseline of less than 150 km in length were taken where the difference between them were about 10 km, and three baselines long length. Table 3 shows these baselines and their Cartesian components in WGS 84 coordinate system. Four days are taken from observation period (110, 112, 114, and 115). With respect to direction, baseline from station HURO to TURO and from KATO to NEKO cover north-south direction, baseline from KATO to DAHO covers east-west direction; the rest baselines cover random directions.

The Weighted Ambiguity Vector Estimator (WAVE) software GPSurvey version 2.00 was used for computation [18]. The following cases are considered in the analysis; comparing the use of Broadcast ephemeredes with precise ephemeredes, using Model for troposphere or ignoring it.

The baseline length with its standard deviation and the components of the baseline with their standard deviations are the main concern in this analysis. For all figures below, the following notations are used:

H for Hopfield model,
B for Broadcast ephemeredes,
P for Precise ephemeredes,
N for Ignoring troposphere model,

4.1.2 Precise ephemeredes and broadcast ephemeredes

The effect of using the precise ephemeredes and broadcast ephemeredes which emitted with the satellite message on the standard deviation in (mm) for different baseline lengths are shown by the scatter diagrams of in fig. 3.

Table 2
Approximate coordinates of the GPS stations (in WGS 84)

Coordinates / Station	Latitude	Longitude	Ellipsoid height
HURO	27° 22` 26.95" N	33° 37` 37.02" E	49.37
GHAO	28° 41` 48.57" N	32° 49` 15.40" E	22.30
DARO	29° 22` 43.26" N	32° 33` 56.27" E	23.20
RAHO	29° 59` 24.51" N	32° 52` 09.80" E	308.39
ZENO	29° 08` 28.38" N	33° 06` 08.49" E	146.77
KATO	28° 43` 20.83" N	33° 47` 24.77" E	915.59
TURO	28° 16` 09.71" N	33° 35` 46.73" E	121.52
MOHO	27° 50` 46.95" N	34° 11` 01.47" E	249.32
DAHO	28° 44` 52.58" N	34° 28` 02.05" E	557.65
NEKO	29° 57` 50.64" N	33° 44` 34.84" E	456.51
GENO	30° 10` 30.44" N	32° 25` 57.67" E	60.95
ISMO	30° 36` 56.53" N	32° 19` 07.03" E	35.47

Table 3
Baselines lengths and their components (absolute value)

Baseline		Length	d X	d Y	d Z	d N	d E	d U
From	To	(m)	(m)	(m)	(m)	(m)	(m)	(m)
GHAO	ZENO	56383	34823	10125	43172	49220	27500	374
KATO	DAHO	66204	38493	53814	2305	3012	66132	701
HURO	MOHO	75890	50640	32188	46462	52452	54845	252
RAHO	NEKO	84365	44984	71330	2429	2569	84325	409
HURO	TURO	99250	36836	28108	87770	99200	3030	847
ZENO	NEKO	110340	71523	27191	79498	91380	61839	647
KATO	NEKO	137711	53853	41520	119750	137622	4556	1951
GHAO	MOHO	163585	36411	136242	82900	93483	134229	1872
DARO	MOHO	232114	18973	176983	148976	168707	159370	4005
HURO	DARO	245285	31667	144795	195438	221632	104984	4706

Fig. 3-a shows the results for two cases mentioned above. From fig. 3-a it can be noticed that all values of standard deviations are below 1 mm for most baselines but only two baselines are above this value. These two baselines were observed on day 112, the first one between station NEKO and RAHO and the other between NEKO and ZENO. The reason may be noticed from table 4 as the station start time begins after the defined time by 1 hour and 40 minutes than other stations. So, the data used in processing is less than the others for all baselines in the network.

Fig. 3-b, 3-c and 3-d show the relationship between standard deviation and the baseline components in three directions X-direction, Y-direction and Z-direction. The first look to these figures reveals that the component in X-direction has higher standard deviation with respect to other components. This may be due to the fact that satellite trajectory in this region is nearly parallel to the X -direction. An error in the satellite orbit may be divided into three components along track (direction of motion), radial (direction from satellite to earth) and across track (perpendicular to the other two). Due mainly to difficulties in modeling solar radiation pressure, the along - track error is the greatest of the three. Many authors reported that the error in the along track direction is the biggest one, this means x-direction [19].

Table 4 summarizes the results, obtained for all baselines in two cases and the difference between the baseline lengths. A first glance at table 4 reveals that all baselines obtained using precise ephemeredes are longer than the others by broadcast ephemeredes. These differences are ranging from 1 mm to 28 mm for baselines' length equal to 99250.586 m and 245285.506 m, respectively.

North, east and upper (vertical) components with their standard deviation are shown in figs. 3-e, 3-f and 3-g. The standard deviation scatters are equal to 1 mm or less for north and east components unless the same baselines mentioned before connecting station NEKO with RAHO and ZENO. This is since their scatters are 1.6 mm and 1.1 mm for north components and 1.4 mm and 1.1 mm for east components. Fig. 3-g indicates that upper components are affected comparatively twice larger than the other components.

Table 4
Baselines' lengths using two types of ephemeredes

Stations from- to	V_P (m)	V_B (m)	$V_P - V_B$ (m)
GHAO- ZENO	56383.279	56383.277	0.002
KATO-DAHO	66204.215	66204.208	0.007
HURO-MOHO	75890.53	75890.526	0.004
RAHO-NEKO	48365.862	84365.859	0.003
HURO-TURO	99250.586	99250.585	0.001
ZENO – NEKO	110340.307	110340.304	0.003
KATO-NEKO	137711.509	137711.506	0.003
GHAO-MOHO	163585.731	163585.713	0.018
DARO-MOHO	232114.436	232114.415	0.021
HURO-MOHO	245285.506	245285.478	0.028

V_P is the baseline calculated by using precise ephemeredes in meters,
V_B is the baseline calculated by using broadcast ephemeredes in meters.

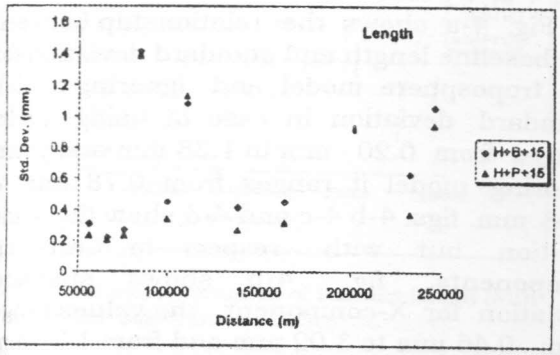

Fig. 3-a. Standard deviation of baseline length (with two ephemeredes types).

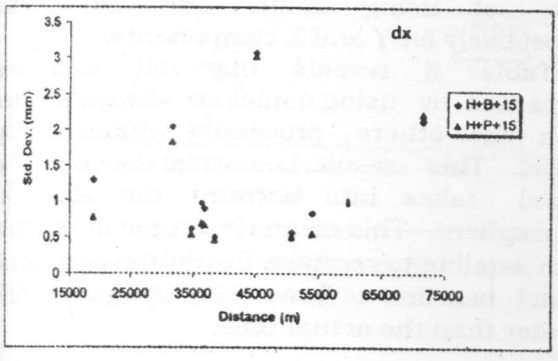

Fig. 3-b. Standard deviation of dX component (with two ephemeredes types).

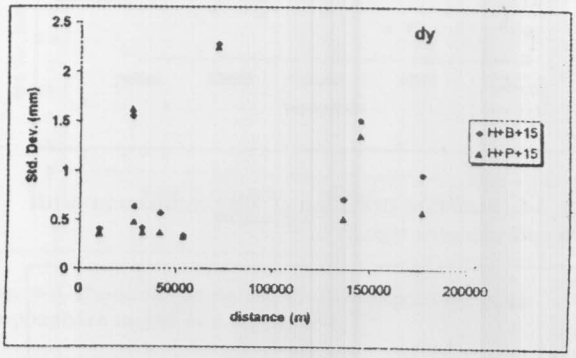

Fig. 3-c. Standard deviation of dY component (with two ephemeredes types).

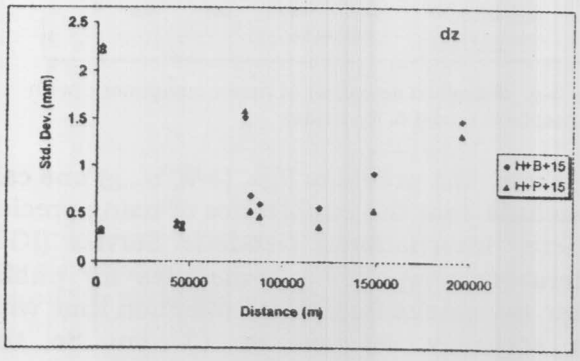

Fig. 3-d. Standard deviation of dZ component (with two ephemeredes types).

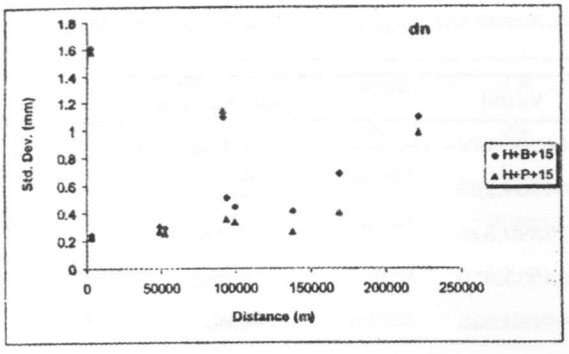

Fig. 3-e. Standard deviation of north component (with two ephemeredes types).

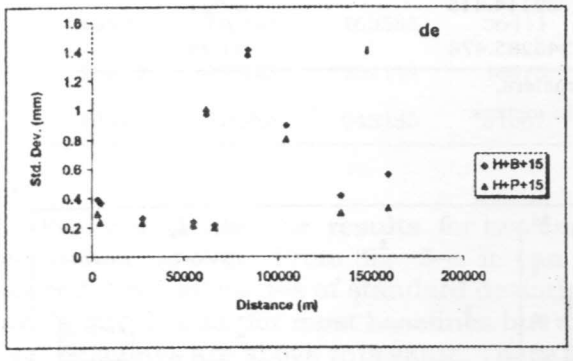

Fig. 3-f. Standard deviation of east component (with two ephemeredes types).

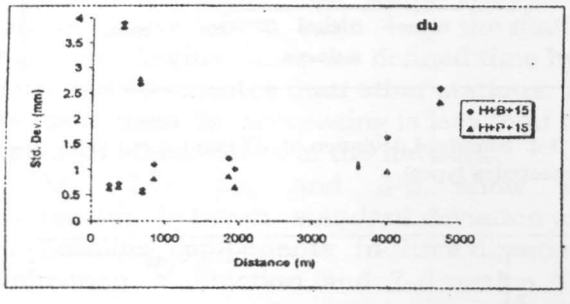

Fig. 3-g. Standard deviation of upper component (with troposphere model & No mode).

From the previous figs. (3-a, b...g) one can conclude that the importance of using precise where International Geodetic Service (IGS) offers this type of ephemeredes for public after two weeks from data collection time with an accuracy reached to 13 cm. So, the employment of the precise ephemeredes is inevitably requested for these ranges of baselines.

4.1. 3. Troposphere model and no model

GPS processing software generally gives a choice of correction model to be used. For example, the GPSurvey package by the Trimble Navigation Limited Company gives a choice of Hopfield, Saastamonen, Good-Godman, Black and no model. Models available gives the same standard deviation values, because it is based on the same theoretical laws; they assume spherical layers, symmetrical refractivity with respect to zenith direction, no temporal change in refractivity and an effective height for the dry layer of about 40 km [2]. Therefore, data will be processed by using Hopfield model and a comparison between using models or ignoring it will be made. The results are shown in figs. 4-a, 4-b, 4-c and 4-d.

Fig. 4-a shows the relationship between the baseline length and standard deviation for the troposphere model and ignoring model. Standard deviation in case of using model ranges from 0.20 mm to 1.38 mm and when ignoring model it ranges from 0.78 mm to 2.68 mm. figs. 4-b 4-c and 4-d show the same relation but with respect to Cartesian components. fig. 4-b shows standard deviation for X-component, the values range from 0.46 mm to 3.02 mm and from 1.71 mm to 5.48 mm for case of using model and no model respectively. Figs. 4-c and 4-d show standard deviation, its range from 0.32 mm to 2.25 mm and from 1.23 mm to 4.03 mm for case of using model and no model respectively for Y and Z components.

Table 5 reveals that all baselines processed by using model are always shorter than the others processed without using model. This result is normal because the model takes into account the effect of troposphere. This means less time for signals from satellite to receiver. But in the case of no model baseline is processed by using time greater than the actual time.

Table 5
Baselines' lengths using troposphere model and ignoring it

Baseline from-to	V_m (m)	V_n (m)	$V_m - V_n$ (m)
GHAO-ZENO	56383.279	56383.277	-0.087
KATO-DAHO	66204.215	66204.301	-0.086
HURO-MOHO	75890.530	75890.659	-0.129
RAHO-NEKO	84365.862	84366.009	-0.147
HURO-TURO	99250.586	99250.749	-0.163
ZENO-NEKO	110340.310	110340.430	-0.119
KATO-NEKO	137711.509	137711.708	-0.199
GHAO-MOHO	163585.731	163586.053	-0.322
DARO-MOHO	232114.436	232114.708	-0.272
HURO-MOHO	245285.506	245285.847	-0.341

V_m is the baseline calculated using Hopfield model and V_n is the baseline calculated without using model.

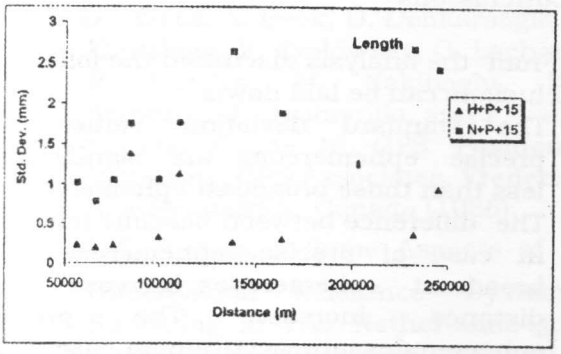

Fig. 4-a. Standard deviation of baseline length (with troposphere model and no model).

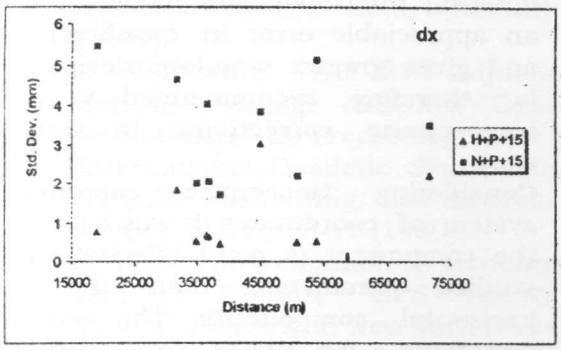

Fig. 4-b. Standard deviation of dX component (with troposphere model and no model).

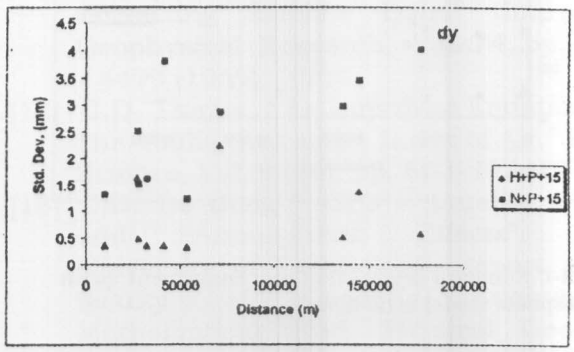

Fig. 4-c. Standard deviation of dY component (with troposphere model and no model).

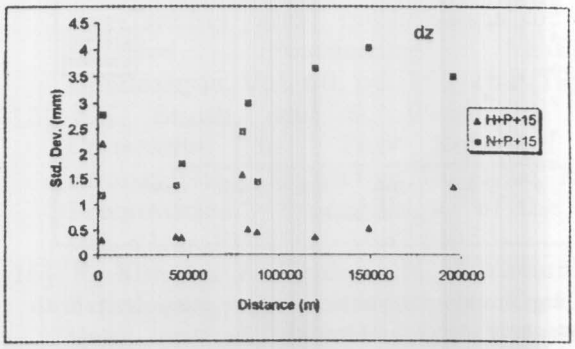

Fig. 4-d. Standard deviation of dZ component (with troposphere model and no model).

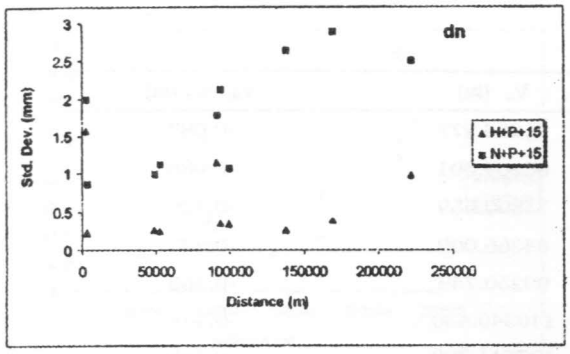

Fig. 4-e. Standard deviation of north component (with troposphere model & no model).

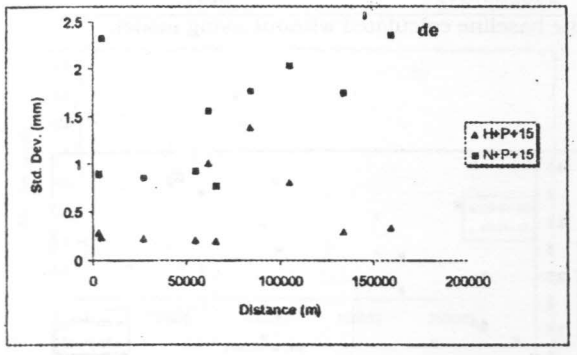

Fig. 4-f. Standard deviation of east component (with troposphere model & no model).

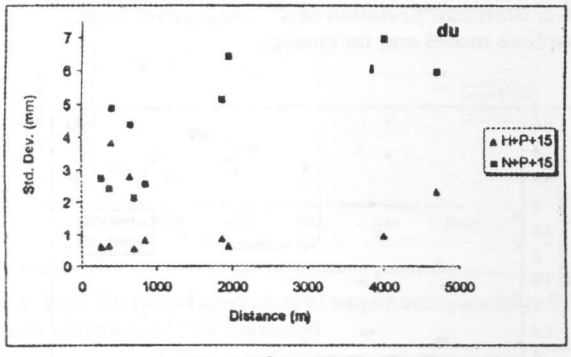

Fig. 4-g. Standard deviation of upper component (with troposphere model & no model).

North, east and Upper (vertical) components with their standard deviation are shown in figs. 4-e, 4-f and 4-g. The standard deviations for the north components are 0.23 mm, 1.58 mm in case of using troposphere model and 0.83 mm, 2.89 mm in case of no model. The standard deviations for East components are 0.20 mm, 1.39 mm in case of using troposphere model and 0.77 mm, 2.36 mm in case of ignoring it. The Upper components and their standard deviation are shown in fig. (4-g). Standard deviation ranges for troposphere model from 0.57 mm to 3.83 mm, and ranges from 2.11 mm, 6.98 mm in case of ignoring model.

From figs. (4-a to g) there is a significant difference between standard deviation when using tropospheric model "Hopfield" and no model. So, using model is requested. No model causes error in the baseline length and its components.

5. Conclusions

From the analysis discussed the following conclusions can be laid down:

- The standard deviation values of precise ephemeredes are significantly less than those broadcast ephemeredes.
- The difference between baseline length in case of precise ephemeredes and broadcast ephemeredes increases with distance increase. The precise ephemeredes are accurate to use in all baseline ranges. It can be concluded, that precise ephemeredes are more reliable than broadcast ephemeredes.
- Ignoring the troposhpere model causes an appreciable error in baseline length and gives greater standard deviation. It is, therefore, recommended to apply tropospheric corrections in accurate work
- Considering Geocentric coordinate system of coordinates, It was found that the component is more affected by the studied parameters than the other horizontal components. The standard deviations for upper components in broadcast ephemeredes are twice as much as those obtained when using when use precise ephemeredes.

References

[1] R.W. King, E.G. Masters, C. Rizos and A. Stolz "Surveying with GPS." Lecture notes prepared for workshop " Surveying with GPS", University of New South Wales, Sydney, 13-14 May (1985).

[2] Leick, "GPS Satellite Surveying". John Wiley & Sons, INC., New York (1995).

[3] D.E. Wells, W. Lindlohr, B. Schaffrin and E. Grafarend " GPS Design: Undifferenced Carrier Beat Phase Observations and the Fundamental Differencing Theorem." Department of Surveying Engineering, Technical Report No. 116, University of New Brunswick, Fredericton, N.B., Canada (1987).

[4] D. Wells, N. Beck, D. Delikaraoglou, A. Kleusberg, E. Krakiwsky, G. Lachapelle, R. Langley, M. Nakiboglu, K. P. Schwarz, J. Tranquilla, and P. Vanicek " The Guide to GPS Positioning". Canadian GPS Associates, Fredericton, New Brunswick, Canada (1986).

[5] J.M. K sters, " Some Aspects of A 3-Dimensional Reference System for Surveying in The Netherlands Quality Analysis of GPS Phase observations". Contract research to: Triangulation Department, Cadastral Service, Apeldoorn and Survey Department, Rijkswaterstaat, Delft, Netherlands (1992).

[6] G. Wübbena, "The GPS Adjustment Software Package -GEONAP- Concepts and Models." In: Proceeding of the Fifth International Geodetic Symposium on Satellite Positioning, Las Cruces, New Mexico, March 13-17 (1989).

[7] B. Hofmann-Wellenhof, H. Lichtenegger, and J. Collins, "GPS Theory and Practice." Springer, New York (1994).

[8] G. Lachapelle, B. Wanless, H. Janes, R. Leeman, E. J. Krakiwsky, K. Schwarz, E. Cannon, K. Pointon, M. Craymer, A. Kleusberg, R. B. Langley, P. Vanicek and D. Wells "Design of General Software Structure for The Processing, Statistical Analysis, and Quality Control of GPS Networks." Geodetic survey of Canada. Contract Report No. 88-002 (1988).

[9] H.S. Hopfield, "Tropospheric Effect On Electro magnetically Measured Range: Prediction From Surface Weather Data." Radio Science, Vol. 6 (3), pp. 357-367 (1971).

[10] H. S. Hopfield, Tropospheric Correction of Electromagnetic Ranging Signals to A Satellite A Study of Parameters". Paper presented at Symposium on electromagnetic distance measurement and the influence of atmospheric refraction, International Association of Geodesy, Wageningen, The Netherlands, 23-28 May (1977).

[11] H. S. Hopfield, "Two-Quartic Tropospheric Refractivity Profile for Correcting Satellite Data." Journal of Geophysical Research, Vol. 74, pp. 4487 – 4499 (1969).

[12] G.D. Thayer, " An Improved Equation for The Radio Refractive Index of Air." Radio Science, Vol. 9 (10), pp. 803-807 (1974).

[13] C.D. De Jong " GPS - Satellite Orbits and Atmospheric Effects". Delft University of Technology. Report of the faculty of Geodetic Engineering, Mathematical and Physical Geodesy, Delft, The Netherlands (1991).

[14] H.W. Janes, R. B. Langley and S. P. Newby "Analysis of Tropospheric Delay Prediction Models: Comparisons with Ray-Tracing and Implications for GPS Relative Positioning." Bulletin Geodesique, Vol. 65, pp. 151-161 (1991).

[15] E.K. Smith, and S. Weintraub "The Constants in The Equation for Atmospheric Refractive Index at Radio Frequencies." Proceedings of the IRE, Vol. 41(8), PP. 1035-1037 (1953).

[16] F. Kimata, A. Tealeb, H. Murakami, N. Furukawa, S. Mahmoud, H. Khalil, K. Sakr and A. M. Hamdy "The Aqaba Earthquake of November 22, 1995 and Co-Seismic Deformation in Sinai Peninsula, Deduced From Repeated GPS Measurements." Acta Geod. Geoph. Hung., Vol. 32 (1-2), pp. 53-71 (1997).

[17] M.S. Abd El- Gelil, " Studying Different Effects on the Geodetic Measurements by Using GPS, For Monitoring crustal Deformations", M.Sc. Thesis, Alexandria University, Faculty of Engineering, Egypt. (1998).

[18] Trimble Navigation "WAVE Software User's Guide." Trimble Navigation Limited. Surveying and Mapping Division. Sunnyvale, California, USA (1995).

[19] G. L. Robinson, "Verification of Gravimetric Geoidal Models by a combination of GPS and Orthometric Height." M. Sc. E. thesis, Department of Surveying Engineering. Technical Report No. 152, University of New Brunswick, Fredericton, Canada (1991).

Received September 15, 2000
Accepted December 7, 2000